SOILS AND FOUNDATIONS Vol. 45, No. 6, 15–30, Dec. 2005
Japanese Geotechnical Society

SOFT GROUND IMPROVEMENT BY VERTICAL RIGID PILES TWO-DIMENSIONAL PHYSICAL MODELLING AND COMPARISON WITH CURRENT DESIGN METHODS

ORIANNE JENCK[i], DANIEL DIAS[i] and RICHARD KASTNER[i]

ABSTRACT

Soft soil improvement by vertical rigid piles permits reduction and homogenization of settlements under structures. This process provides an economic and effective solution, especially when rapid construction is required. The field applications are mainly roadways, railways and industrial building foundations. Piles are installed into the soft soil and rest on a substratum, which is a more rigid layer. Loads applied on surface are transferred to the pile caps, thanks to a granular mat, added on the soft layer, in which arching occurs. This paper describes the main features of the improvement and summarizes several calculation rules for the design. Some physical models of piled earth platform from the literature are presented. A two-dimensional small scale model was developed and some experimental results are presented. The granular soil mat is modelled by the two-dimensional Taylor-Schneebeli analogical material, the soft soil is modelled by foam and the piles are modelled by metallic elements. The instrumentation permits the analysis of the load transfer on piles and an image correlation method permits the analysis of the displacement fields in the model. The experimental results are compared to several current calculation methods.

Key words: arching effect, design method, physical modelling, piled embankment, soil improvement (**IGC**: E2/E14/H1)

INTRODUCTION

Ground improvement through vertical rigid piles is an interesting alternative method for foundations on soft soils. This process is being used more and more to improve soil foundation for railways, roadways, industrial pavements, storage tanks and wastewater treatment plants (Barry et al., 1995; Liausu and Pezot, 2001; Cortlever, 2001; Alexiew and Vogel, 2002; Zanziger and Gartung, 2002; Wood, 2003). The aim of this technique is to improve a soft soil layer that would lead to great settlements which would harm the normal function of the structure and its durability.

The load applied by the structure is transferred to the substratum, which is a more rigid layer, through a granular mat built on the soft soil layer reinforced by a vertical rigid pile grid. Arches are developed in this load transfer mat, permitting the load to be transferred onto the piles. Friction along the piles is also involved in the improvement mechanism, leading to a complex soil/structure interaction phenomenon. This technique is different from those of classical piles because piles are not directly connected to the structure.

This improvement technique can be an interesting alternative to more traditional methods like preloading, vertical drains, electro-osmosis, injection or lightweight fill; it is fast and it does not necessitate the soft soil replacement (Magnan, 1994).

The precise load transfer mechanisms developed in the granular mat and along the piles remain poorly understood. While several design methods exist, most of them consider independently the mechanisms developed in the load transfer mat and in the reinforced soft soil layer, and none can yet take into account the complex behaviour of the full system.

Guidelines do not yet exist in France for this technique of soil improvement. A French national research project (''Inclusions Rigides'') is starting to address this problem. A state of the art report has been completed by Briançon (2002) and a numerical feasibility study presented by Laurent et al. (2003). The aim of this project is to edit the guidelines of design, construction and control of ground improvement systems by vertical rigid piles.

Our contribution to the study of the load transfer mechanisms taking place in the granular mat consists of a physical model. The model is two-dimensional and uses the Schneebeli's analogical soil to simulate the granular mat material. Foam elements are used to model the soft soil and metallic elements represent the rigid piles. An instrumentation permits the analysis of the load transfer on pile caps and an image correlation method permits the analysis of the displacements in the model. A parametric

[i] URGC Géotechnique-INSA de Lyon, France (orianne.jenck@insa-lyon.fr).
The manuscript for this paper was received for review on October 13, 2004; approved on September 6, 2005.
Written discussions on this paper should be submitted before July 1, 2006 to the Japanese Geotechnical Society, 4-38-2, Sengoku, Bunkyo-ku, Tokyo 112-0011, Japan. Upon request the closing date may be extended one month.

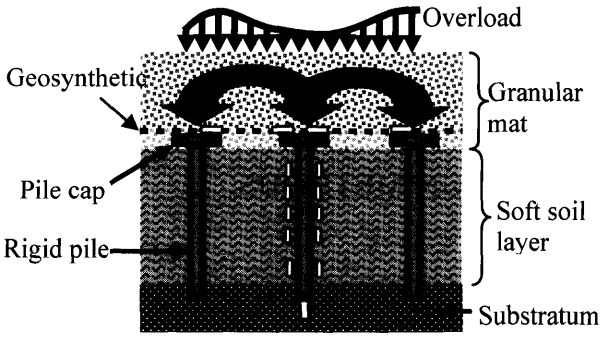

Fig. 1. Rigid pile improvement principle

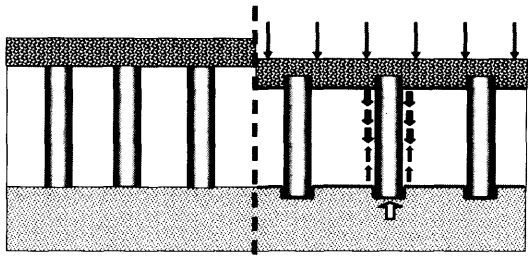

Fig. 2. Friction along the piles when subjected to a surface load, after Berthelot et al. (2003)

study was performed, varying the capping ratio and the mat height, in order to highlight their influence on load transfer and on surface settlement reduction. The results obtained by the physical model are compared to those of the current design methods, which have been adapted to two-dimensional cases.

PRINCIPLE OF THE SOIL IMPROVEMENT BY PILES

The principle of soft soil improvement by vertical rigid piles is represented in Fig. 1. Surface load is transferred to a substratum below the soft soil layer due to the association of a granular mat placed between the structure and the improved soft soil layer, and a rigid pile grid constructed into the soft ground layer.

The mat is made of gravel, ballast or coarse soil and aims at transferring the load applied on its surface. The soft foundation material settles, then consolidates, and differential displacement occurs between the rigid piles and the soft soil. Shear stresses are generated in the granular mat material, creating arches that transfer the stress from soft foundation material onto the piles. Arching takes place only if the mat height is sufficient (Rathmayer, 1975). Moreover, it seems that several mat material parameters play a role in arching (friction angle; dilatancy; particle size; non linear behaviour, etc.). The arches enable load transfer to piles, homogenization and reduction of surface settlements. The area covered by the piles can be increased by adding caps. The capping ratio α is the proportion of the surface covered by the pile caps, and currently lies in a range from 10% to 25%.

Basal geosynthetic reinforcement can be added between the mat and the piles and is involved in the load transfer on piles due to the tension induced by the differential settlements.

Friction along the piles is also implicated in this complex soil/structure phenomenon. In the upper part of the piles (Fig. 2), the compressible soil settles more than the piles, leading to negative friction. It contributes to the load transfer on the piles. In the lower part, the piles move into the substratum (which is not perfectly rigid) and settle more than the soft soil, which then leads to positive friction. A toe resistance develops in the lower end anchored in the substratum.

Mechanisms that develop in the granular mat and along the piles strongly interact: the settlements at the interface between the mat and the soft ground govern both the arching effect and the friction along the piles.

Piles can be preformed or manufactured in-situ. The preformed piles can be timber piles, metallic piles or concrete piles. In-situ constructed piles are more particularly bored piles or piles manufactured by soil mixing. Their deformation modulus ranges between 20 MPa (soil mixing) and 200 GPa (steel pile). Most of the piles are actually reinforced concrete pile, with a modulus between 2 and 20 GPa. A detailed list of pile types and installation techniques has been described by Briançon et al. (2004).

The piles are generally installed through the soft soil layer to the substratum. The pile grid and pile diameter are designed taking a factor of safety against bearing capacity failure into account. There are two ways of designing the piles:

—They are supposed to carry the total mat weight and overload, more particularly when a basal reinforcement is incorporated, which is supposed to transfer the rest of the mat load that is not transmitted through arching. In this case the soft subsoil support is totally neglected (Collin et al., 2005).

—The soft subsoil supports part of the load, even when basal reinforcement is incorporated, and the foundation system can then be optimized (Habib et al., 2002; Russel and Pierpoint, 1998; Rogbeck et al., 1998). The soft soil settlement and consolidation should then be taken into account.

DESIGN METHODS

Most of the design methods aim at estimating the load distribution at the mat base, generally in order to design a layer of geosynthetic reinforcement (BS 8006, 1995; EGBEO, 2004). These methods assume that an important part of the load is transferred to the piles, due to arching and geosynthetic reinforcement. The effect of the soft subsoil reaction is rarely taken into account, whereas the mechanisms developing above the piles and in the soft subsoil are connected. Only the Combarieu method can be qualified as "global", because it considers the soft subsoil and can be used to design the piles.

In the following section, the most relevant methods used in practice are presented. The methods are based on:

—Marston and Anderson (1913) concept

—Terzaghi (1943) concept
—Vault model
—Negative friction theory

British Standard (BS 8006, 1995)

The method used in BS 8006 (1995) was initially developed by John (1987) and Jones et al. (1990). BS 8006 (1995) estimates the load distribution at the mat base by using the Marston and Anderson (1913) concept: soil arching between adjacent pile caps induces greater vertical stresses on the pile caps than on the surrounding soft soil. The average pressure acting on pile cap (q_p) is given by;

$$\frac{q_p}{\gamma \cdot H_M} = \left(\frac{C_c \cdot a}{H_M}\right)^2 \quad (1)$$

where

a: pile cap width,
H_M: mat height,
C_c: arching coefficient:
$C_c = 1.95 \cdot (H_M/a) - 0.18$ for end-bearing piles,
$C_c = 1.55 \cdot (H_M/a) - 0.07$ for frictions piles.

The Marston's original formula, which was for loading on an infinitely long pipe, has been squared, in order to take into account the three-dimensional situation. It seems questionable (Love and Milligan, 2003) that this assumption fully captures the complexity of the 3D situation. In two dimensions q_p would be given by:

$$\frac{q_p}{\gamma \cdot H_M} = \frac{C_c \cdot a}{H_M} \quad (2)$$

BS 8006 recommends installing a geosynthetic reinforcement at the base of the mat, in order to transfer the rest of the load onto the pile caps. However, the load transfer mechanisms with an arching effect and a membrane tension are treated independently. It is assumed that no load is carried directly by the soft subsoil, whereas Jones et al. (1990) highlighted the importance of partial soft soil support.

A limit of this standard is that the mat strength characteristics are not directly taken into account; they are included in the empirical arching coefficient C_c.

The standard defines a critical mat height $H_c = 1.4(s\text{-}a)$, where s is the pile spacing. The weight of the soil above H_c and the surface load are both completely transferred to the pile caps; the soil weight of the area below the arch has to be supported by the geosynthetic membrane. If the height of the mat is less than H_c, complete arching can not occur and the surface load has to be supported by the membrane.

To ensure that differential settlements can not occur at the surface of the mat, BS 8006 recommends a minimum mat height of $0.7(s\text{-}a)$.

In the literature, several pile embankment sites designed according to this standard are presented. Mankbadi et al. (2004) used BS 8006 to calculate the vertical load supported by the geosynthetic placed on a soft ground improved by vibro-concrete columns, to support an approach embankment. Wood (2003) presents the design of a pile-supported embankment for the A63 Selby bypass in the UK. The geosynthetic was designed using BS 8006, but the determination of the load supported by the geosynthetic using this standard gave inconsistent results, hence another design method was preferred (Hewlett and Randolph method). The piles were designed to support the full load; the pile size is 370 mm or 425 mm diameter, with a net working load of 870 or 1160 kN respectively. The pile spacing ranges between 2.7 m and 3.2 m for embankment heights from 4 m to 9.5 m.

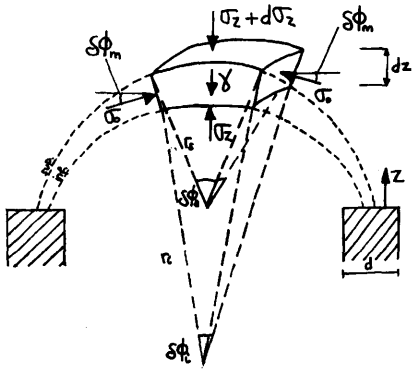

Fig. 3. Arching model proposed by Kempfert et al. (1997)

German Standard (EGBEO, 2004)

The German standard (EGBEO, 2004) is based on a three-dimensional arching model proposed by Kempfert et al. (1997). The vaults rest on the pile caps and lower and upper envelops are not concentric, as shown on Fig. 3.

Two sorts of grids are considered: squared and triangular. A relation giving the average vertical pressure acting on the soft subsoil q_s was obtained by considering soil element equilibrium in the vault axis:

$$q_s = \lambda_1^{\chi} \cdot \left(\gamma + \frac{q_0}{H_M}\right) \cdot \left[H_M \cdot (\lambda_1 + \lambda_2 \cdot h_g^2)^{-\chi} + h_g \cdot \left(\left(\lambda_1 + \frac{\lambda_2 \cdot h_g^2}{4}\right)^{-\chi} - (\lambda_1 + \lambda_2 \cdot h_g^2)^{-\varphi_M}\right)\right] \quad (3)$$

With

$$\lambda_1 = \frac{1}{8}(s_m - d)^2 \quad \lambda_2 = \frac{s_m^2 + 2 \cdot d \cdot s_m - d^2}{2 \cdot s_m^2} \quad \chi = \frac{d \cdot (K_p - 1)}{s_m \cdot \lambda_2}$$

q_0: Surface overload
K_p: Coefficient of passive earth pressure
φ_M: Mat internal friction angle
s_m: Maximal pile spacing
d: Circular pile diameter, for non circular pile $d = d_E = (\sqrt{4A_P/\pi})$, where A_P is the pile section
For $H_M \geq (s_m/2)$, $h_g = (s_m/2)$ otherwise $h_g = H_M$

For a convenient arching effect, a minimum mat height of $s_m/2$ is recommended. Moreover, it is advised that $d/s_m \geq 0.15$.

EGBEO (2004) recommends laying a geosynthetic reinforcement but the arching effect and the membrane

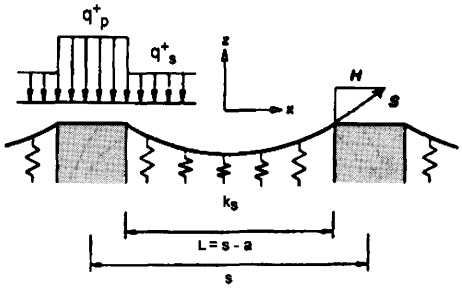

Fig. 4. Subsoil reaction in EGBEO (2004) method

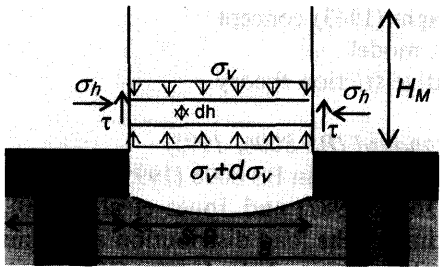

Fig. 5. Terzaghi method

tension are dissociated. A calculation chart is available to design the geosynthetic reinforcement according to the applied load on it, its stiffness, the soft soil support and the width and spacing of piles.

Even if the subsoil support is included (Fig. 4), this method cannot be considered as global, because nothing is said about the grid and pile design.

This method cannot be applied to our study because it is fully three-dimensional.

Terzaghi Method, Adapted by Russel and Pierpoint (1997)

Terzaghi (1943) generalized the Marston's concept by assessing that 'arching is one of the most universal phenomenon encountered in soils both in the field and the laboratory'. He used this concept to determine the behaviour of a soil mass subjected to a differential movement at its base by writing the equilibrium of a soil element of width (*s-a*) and height *dh* (Fig. 5). The stress at the base can be determined by integrating the equilibrium equation. This method has been adapted by Russell and Pierpoint (1997) and Russell et al. (2003) to the three-dimensional problem of piled embankment. In this case, the sliding mass is assumed to have a cruciform section. The plane of equal settlement is considered to be at the mat surface. In the two-dimensional example, the sliding mass has a width of (*s-a*), where (*s-a*) is the distance between two pile cap edges (Fig. 5). The average vertical stress acting on the soft soil is then given by:

$$q_s = \frac{\gamma \cdot (s-a)}{2 \cdot K_a \cdot \tan \varphi_M} \cdot \left(1 - \exp\left(-2 \cdot K_a \cdot \tan \varphi_M \cdot \frac{H_M}{s-a}\right)\right) \quad (4)$$

Where K_a is the coefficient of active earth pressure.

Handy (1985) proposed that the shape of the arched soil is a catenary and suggested the use of the coefficient K_w instead of K_a, in order to take account of the new principal stress orientation, as explained by McKelvey III (1994):

$$K_w = 1.06 \cdot \left(\cos^2\left(\frac{\pi}{4} + \frac{\varphi_M}{2}\right) + K_a \cdot \sin^2\left(\frac{\pi}{4} + \frac{\varphi_M}{2}\right)\right) \quad (5)$$

Habib et al. (2002) compared the results obtained on a monitored site in the Netherlands (widening of a road founded on a geogrid reinforced mattress on piles) with different design methods. Terzaghi method gave the most adequate results, whereas BS 8006 and Hewlett and Randolph methods underestimated the arching effect.

Hewlett and Randolph Method, Modified by Low et al. (1994)

Hewlett and Randolph (1988) idealised the arching of granular fill as a system of vaulted domes of hemispherical shape supported on diagonally opposite pile caps. The two-dimensional example takes into account a semi-cylindrical arch with thickness equal to half the width of a pile cap (Fig. 6(a)). Static equilibrium of vault elements permits calculation of the efficacy E, defined as the proportion of the mat weight carried by the piles. The refinement brought in Low et al. (1994) method consists in considering an empirical coefficient α_R that allows a possible non uniform vertical stress on the soft ground (Fig. 6(b)). Current values for α_R are in the range between 0.8 and 1. The efficacy is given by Eq. (6):

$$E = 1 - \alpha_R \cdot \left(\bar{\omega} + \frac{s}{H_M} \cdot m\right) \quad (6)$$

Where

$$\bar{\omega} = \left(1 - \frac{a}{s}\right)^{K_p}$$

and

$$m = \frac{(K_p - 1) \cdot \left[\left(1 - \frac{a}{s}\right)^2 - \left(1 - \frac{a}{s}\right)^{K_p}\right]}{2 \cdot (K_p - 2)}$$

for

$$H_M/s \geq 0.5$$

Alexiew and Vogel (2002) reported several sites in Germany (railway embankments) where the stress distribution at mat base is calculated using the Hewlett and Randolph method. Moreover, the geosynthetic was designed by taking the subsoil reaction into account, as suggested by Kempfert et al. (1997) in the German standards.

Combarieu Method

Combarieu (1988) proposed a method based on negative friction theory. This method is "global" because it takes into account the soft subsoil reaction. Shearing along concentric cylindrical surfaces centred on the pile is considered both in the mat and the soft ground. Combarieu (1988) assumes that arching effect occurs since the soft subsoil settles more than the piles and columns of soil extending the piles in the mat are sub-

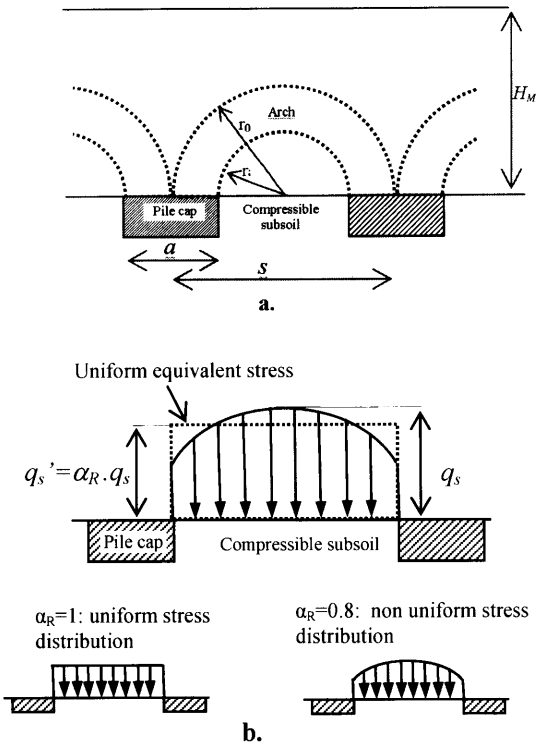

Fig. 6. Analytical model: semi cylindrical sand arches (a)—Equivalent uniform stress acting on soft ground (b)

jected to negative friction.

By applying this method in the mat only and in the particular case of frictional material, this method leads to the same results as Terzaghi (1943) method.

By applying this negative friction model to both the mat and the soft ground, a global method is proposed which permits design of the improvement by rigid piles. Due to negative friction, soft soil will load the piles and the load transfer on piles will be enlarged. Figure 7 illustrates the pile design methodology based on the skin friction theory, as developed by Berthelot et al. (2003): the point where the pile settles as much as the soil corresponds to the neutral point, where the compressive stress in the pile is the larger.

Combarieu method was adapted and completed by Simon (2001). The developments were implemented in the foundation design software FOXTA (2004).

Conclusion on Existing Methods

Several authors have demonstrated that these existing methods of determining the load transfer due to arching yield very different results (Russel and Pierpoint, 1997; Habib et al., 2002; Briançon et al., 2004; Naughton and Kempton, 2004; Stewart and Filz, 2005).

PHYSICAL MODELLING

A number of laboratory controlled investigations have been carried out with the aim of providing a better understanding of the mechanism of piled embankment behaviour and identifying the controlling parameters. Some of these physical models are first presented, with some important results. Secondly, the developed model test is described, and the results from the analysis are given in term of load transfer and displacement field.

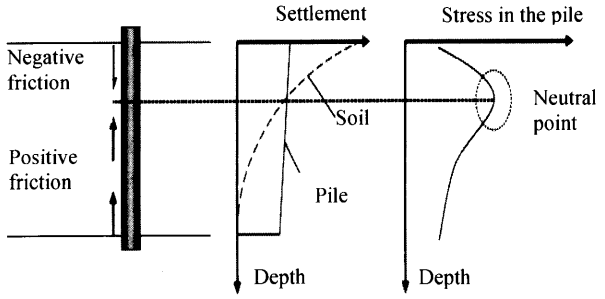

Fig. 7. Friction along the pile, settlements and stress, after Berthelot et al. (2003)

Existing Physical Models

Hewlett and Randolph (1988) performed small scale tests in order to develop an analytical method for calculating load report on piles by arching. They used a bed of foam rubber to model the soft subsoil and the piles were simulated by wooden blocks. By placing sand in alternate colour layers, they observed the mat deformation and the formation of the vaults during the 24 hour foam creeping. The proportion of the weight carried by the piles increased with the number of piles.

Low et al. (1994) investigated the arching in mats on soft ground supported by piles by use of two-dimensional model tests. The piles were simulated by wooden blocks and the soft ground by rubber foam. Friction between the piles and the rubber foam was eliminated: the load cells monitored the total load acting on the soft ground. The following was noted:

—The efficacy (proportion of mat weight supported by the piles) increased with the capping ratio α.

—The competency (ratio between load acting on pile cap and weight of a mat column of same section as pile cap) increased with the pile spacing, and approached a threshold value at large spacing.

—The ratio between the average stress that acts on soft rubber foam and the average stress that acts at the mat base (Stress reduction ratio SRR) was initially equal to 1 and decreased with the increase in the mat height. A constant value was reached for large mat height.

—The stress on the soft ground was lower when the piles were spaced closer.

Demerdash (1996) carried out three-dimensional model tests representing a square grid of individually capped piles. Different pile cap sizes were employed. A movable base was used to model the soft ground, simulating the worst case in which the soft ground was not involved in the load sharing mechanism. Lowering of the mobile platform simulated the yielding of the soft subgrade. Basal geosynthetic reinforcement was incorporated. Two loading procedures were adopted: lowering of the

platform during construction of the mat or after achieving the required height of fill, simulating the post-construction behaviour. This procedure led to a larger load transfer onto piles. The surface settlements were monitored and the tests showed that the differential settlements were reduced when the mat height increased. The controlling parameter seemed to be the mat height normalized by the clear spacing, called depth ratio: $H_M/(s\text{-}a)$. For a depth ratio between 1.7 and 2.0, surface settlement was homogeneous.

Description of the Two-Dimensional Model Test

A laboratory model test has been constructed in order to investigate the influence of several parameters on load transfer mechanisms occurring in the granular mat. The small scale model is two-dimensional and uses an analogical material for the mat. It implies a simplification compared to real structures because of its geometry and analogical soil properties. In fact, this material has a friction angle of 24° compared to 30–40° for a current embankment material. However, this model permits a precise analysis of the influence of several parameters on load transfer mechanisms and permits the development of a database for future numerical analysis. In fact, this model presents a high modularity and basal geosynthetic reinforcement can also be incorporated. Moreover this model allows easy access to the displacement field due to image processing, and easy access to the load distribution at mat base due to instrumentation by load cells: the innovative aspect of this model test is the precise analysis of the results in term of both load and displacements. This permits more robust numerical modelling validation.

The load transfer mat is modelled by the Schneebeli analogical material, which is an assembly of 60 mm long steel rods with diameter of 3, 4 and 5 mm and which constitutes a frictional strongly dilative two-dimensional granular material. Schneebeli (1956) performed two-dimensional compression tests and showed that rod pilings behave like cohesionless soils. It is necessary to use at least two different rod diameters to obtain an isotropic media and the behaviour is then governed by the Coulomb law. The soft soil is modelled by foam and the rigid piles by steel elements. A diagram of the experiment is shown on Fig. 8. Two piles are represented with a pile spacing of length s, and then the model width is $2s$. Vertical walls are lined with Teflon sheets in order to avoid wall friction. These boundaries can then be considered as symmetry planes.

Most of the existing physical models use sand to model the granular mat material, which is actually made of gravel or coarse soil. The analogical soil used in the proposed two-dimensional model test presents several advantages:

—This material is strongly dilative, property which corresponds to dense coarse soils.

—It has a modulus depending on the stress level, property which also concerns gravels (Paute et al., 1994; Valle, 2001).

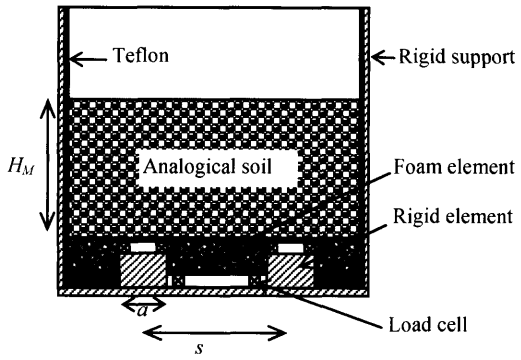

Fig. 8. Schematic view of the experiment

—This material is heavier than a classical soil: its unit weight is equal to 62 kN/m^3. For 1 g modelling, it leads to a reduction of the similarity distortion between model and prototype. In fact, for a scale reduction approximately equal to 3, the stress level is maintained.

—As it is a rod piling, this soil does not necessitate a facial support. The wall friction between soil and support, which is inevitable when using sand, is then totally eliminated.

—Using a rod assembly permits easy access to the displacement field due to image processing: the rods are coloured to obtain contrast and photographs are taken and processed by a numerical image correlation method.

Rods are piled up in 0.10 m layers until a maximum mat height of 0.70 m. An overload constituted by a layer of steel blocks representing a 4.3 kPa surface load is placed on the surface. Creeping of the foam during 80 minutes can qualitatively represent the consolidation of the soft ground and permits the visualization of the displacement field in the whole mass.

Three load cells are placed beneath each pile cap that consists of metallic plates and four load cells are placed beneath a rigid support on which the central foam element rests. This instrumentation permits quantification of the load distribution at the base of the mat but also of the vertical friction between the metallic rigid elements and the soft foam. The total applied load is known due to the knowledge of the analogical soil unit weight of 62 kN/m^3. The load distribution is illustrated on Fig. 9. The weight of a slice of soil of length s is W, F_p is the average load acting on a pile cap, F_s is the load acting on the surface of the foam element, F_b is the load acting at the base of the foam element, directly measured by the cells. F_{fr} is the friction acting on both sides of a pile.

As the similarity between model and prototype is not strictly respected, the experimental results can not be directly extrapolated to real structures. This physical model belongs to the category of models which permits confrontation to design methods and/or calibration of numerical models (James, 1972).

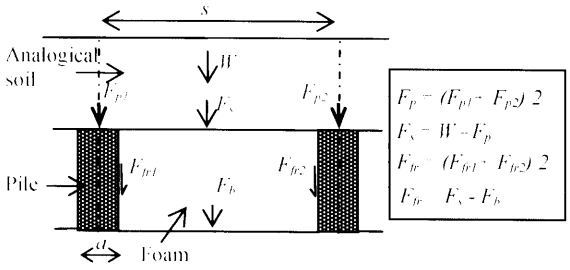

Fig. 9. Load distribution in the model test

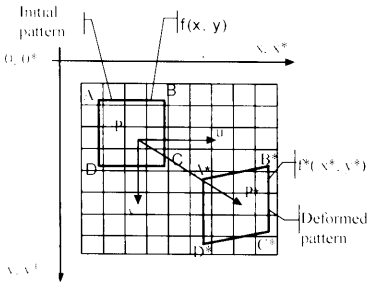

Fig. 10. Image correlation method

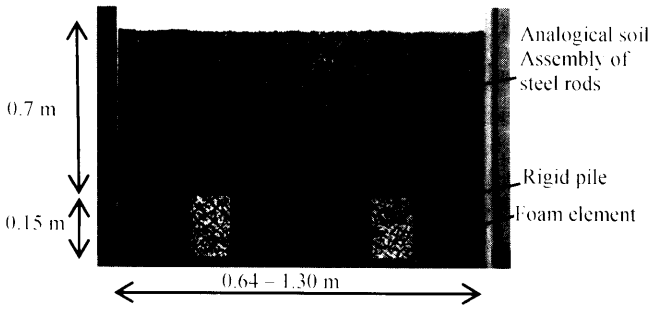

Fig. 11. Physical model

Numerical Imaging

Photographs (Fig. 11) are taken at each loading step and the displacement field in the model is calculated using an image correlation method, implemented in the 'Icasoft' software (Mguil-Touchal et al., 1996). This method compares pixel patterns in an initial and a deformed picture (Fig. 10). The displacement field (u,v) from the initial to the deformed picture is found due to a grey level correlation technique. The grey level function in the initial picture $f(x, y)$ becomes $f^*(x^*, y^*)$ in the deformed picture following:

$$f^*(x^*, y^*) = f^*(x + u\ (x, y), y + v\ (x, y)) \qquad (7)$$

Calculation begins with a reference point where u and v are known and are used to find a minimum correlation coefficient between initial and deformed patterns.

This technique is well adapted to the use of the steel rods, because their face can easily be coloured in order to have contrast (Fig. 11).

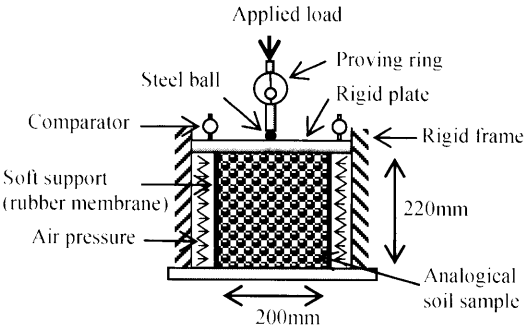

Fig. 12. Biaxial test apparatus

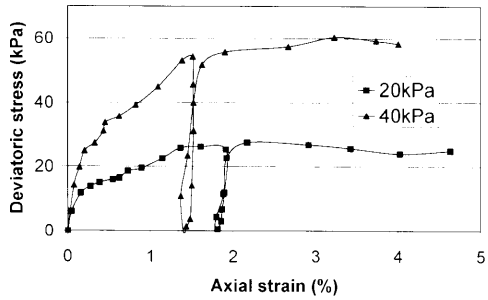

Fig. 13. Stress-strain behaviour

Mechanical Behaviour of the Schneebeli Analogical Soil

Biaxial compression tests at confinement pressures equivalent to those obtained in our model test (20–50 kPa) were performed by Dolzhenko (2002) in order to determine the mechanical behaviour of Schneebeli analogical soil. A diagram of the test apparatus is shown on Fig. 12. A rod assembly sample of 200 mm × 220 mm × 60 mm is confined to a pressure σ_3 through air pressure injected in the rubber membrane. Vertical displacement increments are applied to the upper rigid plate. The corresponding load is measured by a proving ring and the vertical displacement by two comparators. The rigid plate permits repartition of the load on the sample and the steel ball placed between the rigid plate and the piston permits to keep the load centred. Figure 13 depicts the evolution of the deviatoric stress with the axial strain. The deviatoric stress is $\sigma_1 - \sigma_3$, where σ_1 is the vertical applied stress on the sample. No peak is reached before reaching plastic flow. Evolution of volumetric strain with axial strain depicted on Fig. 14 shows a dilative behaviour (negative volumetric strain) from the beginning of the loading. Isotropic compression tests were also performed to complete the parameter identification.

The deviatoric paths reported on the s-t plane (where $s = (\sigma_1 - \sigma_3)/2$ and $t = (\sigma_1 + \sigma_3)/2$) for different confinement pressures permits the determination of the friction angle and the cohesion intercept. The failure criterion defines a line which passes through the origin: cohesion intercept is zero, and with a slope equal to $\sin\phi = 0.41$, then the friction angle ϕ is 24° (Fig. 15).

The following mechanical properties were found out through test results:

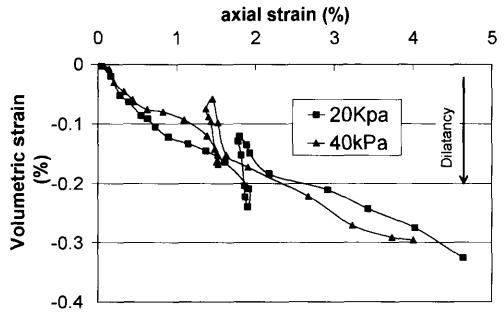

Fig. 14. Volumetric strain versus axial strain

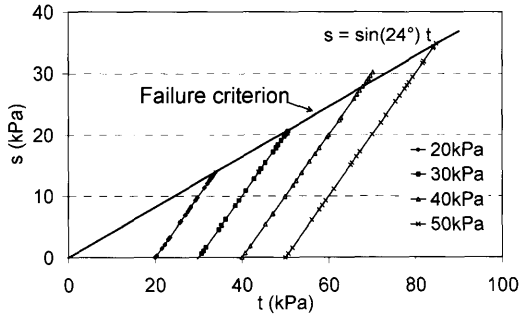

Fig. 15. Deviatoric path in the $s-t$ plane

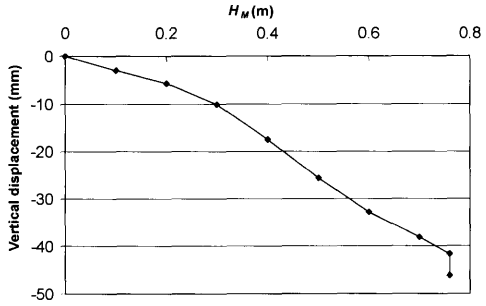

Fig. 16. Vertical displacement according to mat height

—The soil is cohesionless
—The friction angle is equal to 24°
—The dilatancy angle is approximately 4°
—The secant modulus (at 25% of the failure deviatoric stress) varies with the confinement pressure between 25 MPa for $\sigma_3 = 20$ kPa and 47 MPa for $\sigma_3 = 50$ kPa.

Foam Mechanical Behaviour

A foam element was loaded by rods. This test is the reference test and will be used to highlight the influence of the reinforcement by piles. The stress-strain analysis highlights the mechanical behaviour of the foam material. Vertical displacement at foam surface is homogeneous over the element width. It is represented according to the mat height on Fig. 16. The 5 mm vertical displacement on Fig. 16 corresponds to the creep of the foam during 80 minutes. The equivalent vertical stress acting on the foam surface is represented according to the vertical strain on Fig. 17. This curve can be approximated by a bilinear

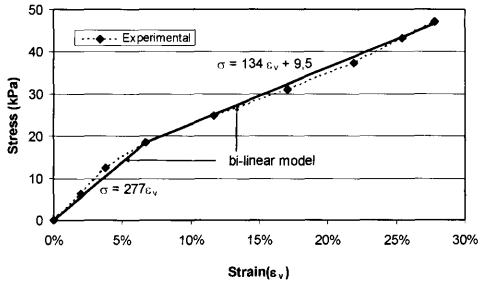

Fig. 17. Vertical strain according to vertical stress

Table 1. Geometrical parameters

a (m)	$s-a$ (m)	s (m)	$\alpha=a/s$
0.1	0.22	0.32	31%
0.1	0.35	0.45	22%
0.1	0.55	0.65	15%

model. Linearization of the curve for strains smaller than 7% gives a modulus of 277 kPa and from a strain of 7%, the linearization gives a modulus of 134 kPa.

Test Results: Embankment Height and Capping Ratio Influence

The geometry of a mat built on soft ground improved by rigid piles is represented by a combination of height of fill H_M, pile cap size a and spacing s. Table 1 summarizes the different test configurations. The cap width is constant ($a=0.1$ m) and the clear pile spacing ($s-a$) varies. In a two-dimensional configuration, the capping ratio is $\alpha=a/s$ and ranges between 15 and 31%.

Figure 18 depicts the results given by the instrumentation. The loads F_p, F_s, F_b and F_{fr} normalized by the weight of the mat (W) are shown according to the mat height, for the three capping ratio values. The normalized load applied on the pile caps increases with the mat height whereas the normalized loads applied on the foam and under the foam decrease. The normalized lateral friction remains relatively constant, but with higher proportion of the mat weight for higher capping ratios. The friction is given in absolute values on Fig. 19. The larger the capping ratio, the larger is the friction along the rigid elements. It should be noted that the lateral friction is much higher in the two-dimensional case as it would be in three dimensions because the contact area between the soft foam and the pile is higher (piles are equivalent to infinite length walls).

Several parameters are used to assess the degree of arching in the granular mat. The efficacy E of the pile support was defined by Hewlett and Randolph (1988) as the proportion of the mat weight carried by the piles:

$$E=\frac{F_p}{W} \tag{8}$$

Where F_p is the load applied on a pile and W the weight of

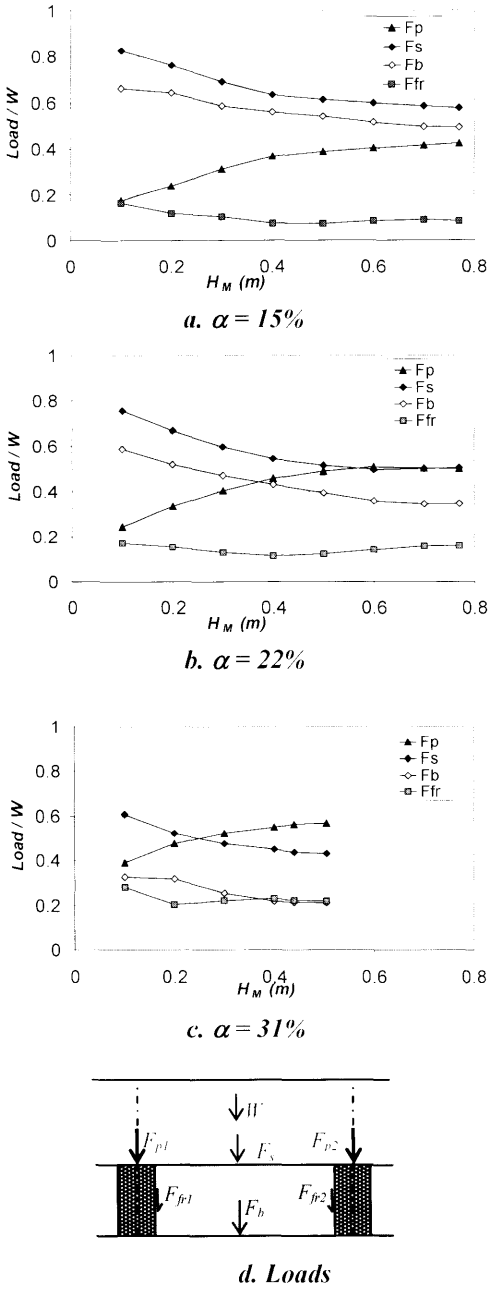

Fig. 18. Results given by the instrumentation

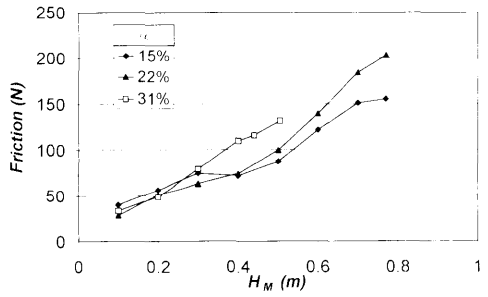

Fig. 19. Friction along lateral boundaries of a "pile"

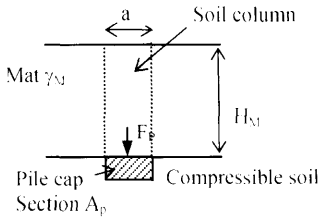

Fig. 20. Competency C

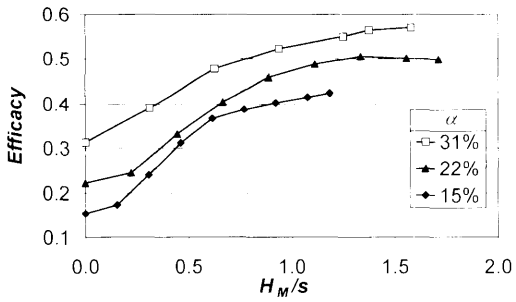

Fig. 21. Efficacy versus depth ratio

a mat slice of length s. This parameter has a value equal to the capping ratio α when there is no arching effect. An alternative is to define the competency C, which is the ratio of the load on the pile cap to the weight of a column of soil having the same width as the pile cap, as shown on Fig. 20:

$$C = \frac{F_p}{H_M \cdot \gamma \cdot A_p} \tag{9}$$

When there is no arching effect the competency is equal to 1. The competency highlights the stress concentration on piles and it is related to the efficacy as:

$$C = \frac{E}{\alpha} \tag{10}$$

The load transfer process is investigated by the variation of the efficacy and the competency versus the depth ratio H_M/s for different capping ratios, as shown on Figs. 21 and 22. Both parameters increase with the mat height. A constant value is reached for a depth ratio of 1.4–1.5 except for $\alpha = 15\%$ where the ultimate mat height reached is not enough. For the same depth ratio, the larger the capping ratio, the larger the proportion of the load carried by the piles, but the lesser the competency: the stress is more concentrated on the pile caps for smaller capping ratios. Increasing the capping ratio from 15% to 31% permits increase of the efficacy by 30% and decrease of the competency by 36%. For $\alpha = 15\%$, the efficacy is increased by 180% compared to the case where no arching occurs ($E = \alpha = 0.15$); for $\alpha = 31\%$, the increase is only by 84%. There might exist an optimum value of α for which the increase in efficacy compared to the case without load transfer onto piles is maximum. For this value of α, the competency would be maximum (maximum ratio $E/\alpha = C$). Figure 23 shows the variation of the efficacy according to the capping ratio. For an increasing capping ratio, the maximum efficacy approaches the α value and for $\alpha = 100\%$, the efficacy is equal to 1.

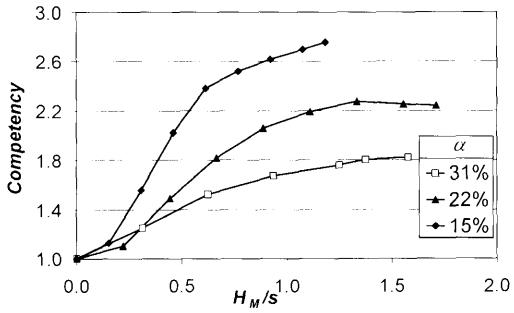

Fig. 22. Competency versus depth ratio

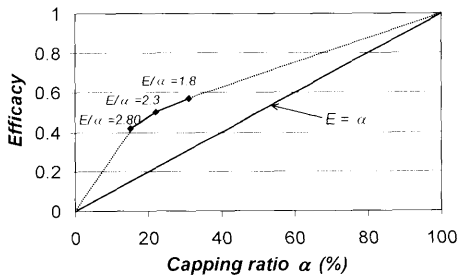

Fig. 23. Maximum efficacy versus capping ratio

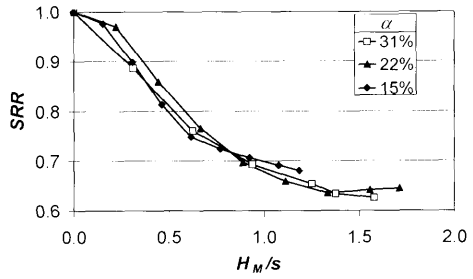

Fig. 24. SRR versus depth ratio

Some authors prefer to define the behaviour of the granular mat by the Stress Reduction Ratio, noted SRR and defined as the ratio of the average vertical stress actually acting on the soft ground (q_s) to the average vertical stress acting at the base of the mat ($q^* = \gamma \cdot H_M + q_0$). SRR is also related to the efficacy and the capping ratio:

$$\mathrm{SRR} = \frac{q_s}{q^*} = \frac{1-E}{1-\alpha} \tag{11}$$

Figure 24 depicts the variation of SRR according to the depth ratio for the three different capping ratios. The SRR is initially equal to 1 and decreases when the depth ratio rises. The SRR reaches a threshold value equal to 0.63. The vertical stress actually acting on the soft foam is only 63% of the stress that would act if there were no improvement by rigid piles. The soft foam is unloaded due to arching effect and a constant value is reached when complete arching occurs. This figure also shows that in this experimentation, the SRR does not depend on the capping ratio when depicted according to H_M/s.

We defined a parameter SRR_m that takes into account the load transfer on the piles by friction between the foam and the piles. SRR_m is the ratio of the average vertical stress acting on the foam support (q_b), directly measured by the load cells, to the average vertical stress q^*:

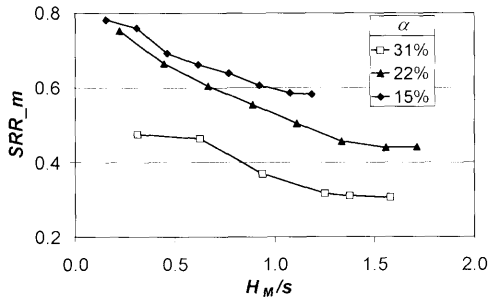

Fig. 25. SRR_m versus depth ratio

$$\mathrm{SRR\_}m = \frac{q_b}{q^*} \tag{12}$$

where $q_b = (F_b/(s-a)\cdot l)$, l is the length of the rods (0.06 m) and $(s-a)$. l is the foam section.

Figure 25 depicts the variation of SRR_m according to the depth ratio for the three different capping ratios. SRR_m decreases when the depth ratio increases: the load is transferred onto the piles and the soft ground is unloaded. SRR_m tends to an ultimate value at important mat height. The larger the capping ratio, the lesser is the SRR_m. In fact, the SRR does not depend on the capping ratio, but, from Fig. 19, the larger the capping ratio, the larger the lateral friction. For $\alpha = 31\%$ and $H_M > 1.4s$ the average stress acting beneath the foam element is only 30% of the stress that would act without improvement.

The degree of soil arching can also be assessed by the reduction of settlement at the base of the mat. The settlements at foam surface can be compared to those obtained without reinforcement for the same mat height. The results are expressed in term of reduction of the settlement compared to the settlement obtained without reinforcement, as explained by the equation:

$$s\% = \left(1 - \frac{s_p}{s^*}\right) \cdot 100 \tag{13}$$

where $s\%$ is the settlement reduction in percentage, s_p is the settlement in the case of pile improvement and s^* in the settlement obtained without reinforcement.

Figure 26(a) presents the settlement reduction for $H_M = 0.44$ m according to the position to the model centre (mid-span between rigid elements) and for three capping ratios. Over the rigid piles, the reduction is always equal to 100% (no settlements). The maximum settlement and thus the minimum reduction is reached mid-span between the piles. The larger the capping ratio, the larger is the settlement reduction. Figure 26(b) depicts the variation of the reduction of the maximum settlement according to the capping ratio for different mat heights. The larger the mat height, the larger is the settlement reduction.

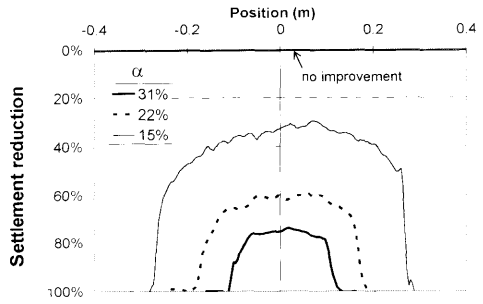

a. settlement repartition for H_M = 0.44 m

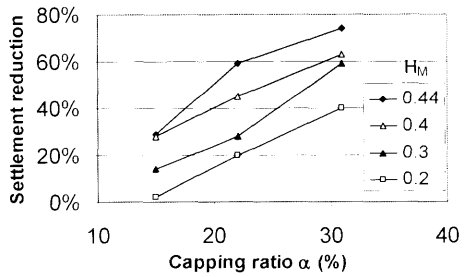

b. Maximum settlement reduction according to α

Fig. 26. Settlement reduction at mat base

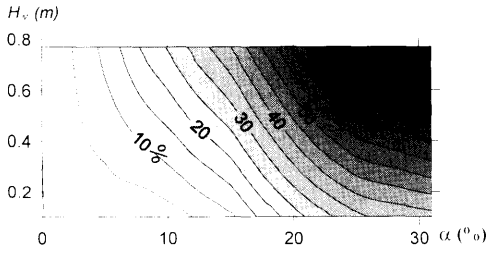

Fig. 27. Settlement reduction (%) at mat base according to α and H_M

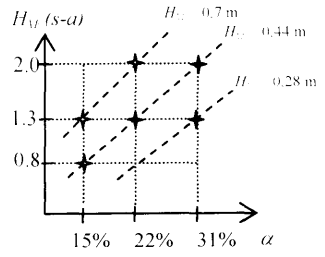

Fig. 28. Parametric study

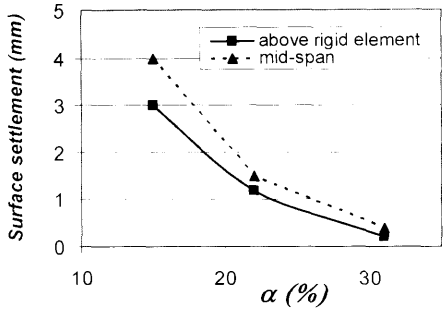

a. According to α for H_M=1.3(s-a)

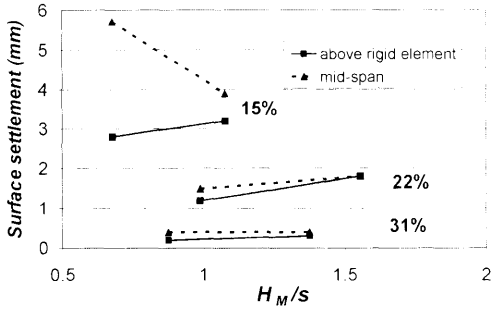

b. According to H_M/s

Fig. 29. Surface settlements during creeping of the foam

Figure 27 highlights the reduction of the maximum settlement reached mid-span between the piles, at the foam surface, according to both H_M and α. For α=0%, there is no reinforcement and thus no settlement reduction. For α<20%, the settlement reduction increases mostly with α and for α>20% the reduction increases with H_M.

At the end of the mat construction, overloads are added on its surface and creeping of the foam during 80 minutes permits simulation of the post-construction behaviour of the structure by simulating consolidation of the soft ground material. During this phase, observation of the displacement field can be made in the whole rod mass. No variation of the load transfer was monitored during this phase, probably because arching was (almost) complete, whereas in their two-dimensional model, Van Eekelen et al. (2003) monitored a pile load increase during consolidation of the foam plastic blocks which simulate the soft soil. In order to study the influence of mat height, tests were performed with creeping of the foam observed at two different values of H_M for each capping ratio. Parametric study can be made either at constant H_M or constant depth ratio $H_M/(s-a)$, as shown on Fig. 28.

Figure 29 depicts the variation of the surface settlement appearing during the creeping period on two points: above a rigid element and mid-span between the piles, according to α and for a mat height of 1.3 $(s-a)$ (Fig. 29(a)) and according to H_M/s, for the three investigated capping ratios (Fig. 29(b)). Both figures clearly show that:

—The differential and the total settlement are reduced with an increasing capping ratio.

—The differential settlement is reduced with an increasing mat height.

—For α=31%, the total and the differential settlement are negligible.

—For α=22%, the required mat height for uniform surface settlement during settlement is approximately 1.5 times the pile spacing s.

—For α=15%, the total and differential settlements are important, but are likely to be reduced with the mat height.

Figures 30 and 31 permit to analyse the mat height influence on the arch formation in the rod assembly for a constant capping ratio α=22%. The creeping of the

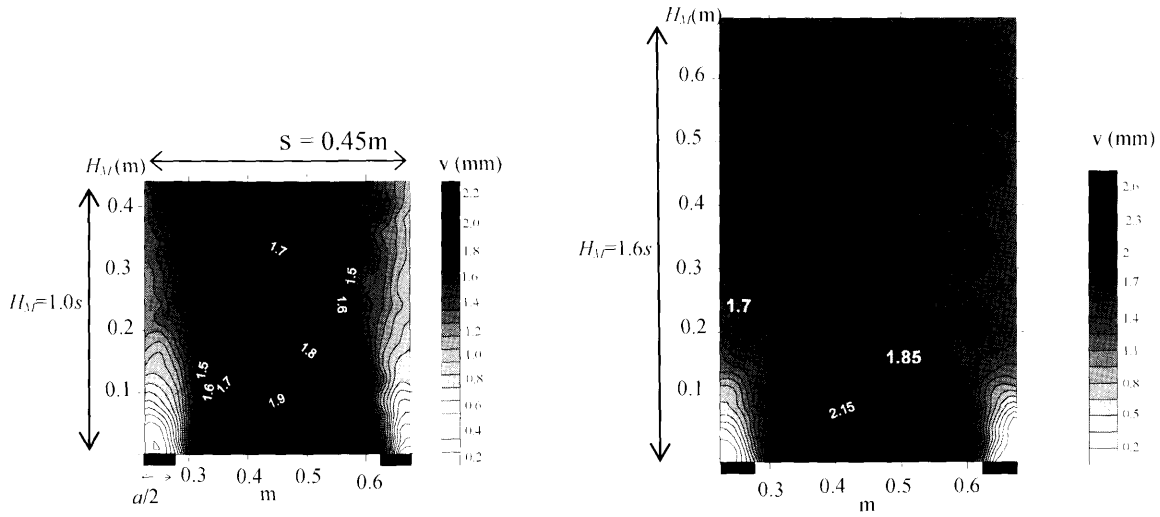

a. H_M=1.0s b. H_M=1.6s

Fig. 30. Vertical displacement in the rod assembly during creeping of the foam for $\alpha = 22\%$

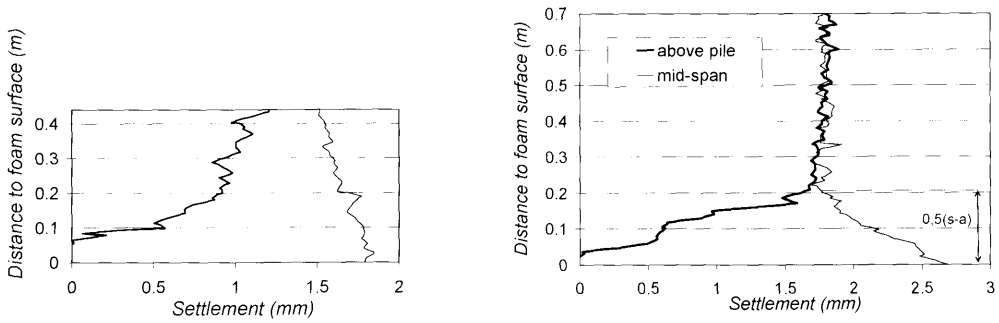

a. H_M = 1.0*s* *b.* H_M =1.6*s*

Fig. 31. Vertical displacement during creeping of the foam for $\alpha = 22\%$, above the pile and mid-span

foam was observed for a mat height of 1.0*s* (Figs. 30(a) and 31(a)) or 1.6*s* (Figs. 30(b) and 31(b)). For the first configuration, a mat height of 0.44 m was reached, the overload (4.3 kPa) was placed on the mat surface and then the creeping is observed. For the second configuration, a mat height of 0.7 m was reached, the overload was added and the creeping is observed. Initial and deformed photographs (beginning and end of the 80 minute foam creeping) are correlated using image processing. The size of the images are approximately 500 pixels × 500 pixels and 600 pixels × 1000 pixels for figure a and figure b respectively. The scale is then 1 pixel = 0.91 mm or 1 pixel = 0.72 mm. The image processing gave the best results for a pattern size of 15 pixels × 15 pixels. The reference point for the processing is chosen on the pile, where there is no displacement. By correlating two successive photographs corresponding to the same state, the precision of the method is determined to approximately 0,03 mm. Figure 30 presents the vertical displacements in the rod assembly that appear during the creeping period, on the width *s* between the piles. This figure shows that there is a vault in the case $H_M = 1.6s$ and the surface settlements are uniform; whereas shear planes extend until the mat surface for $H_M = 1.0s$ and surface differential settlements appear. Figure 31 depicts the variation of this vertical displacement with the distance to foam surface over the pile and mid-span between the piles. This figure shows that there are differential surface settlements for $H_M = 1.0s$, whereas vertical displacements are uniform from a distance of 0.2 m (or 0.5*s*) to the foam surface for $H_M = 1.6s$. This value is lower than $H_M = 1.0s$, for which mat height there is no settlement homogenization: the displacement distribution strongly depends on the presence of fill above this value of 0.5*s*. In a three-dimensional case, the position of the plane of equal settlement would probably change because of the vault configuration (3D) and the increase of the friction angle value.

Figure 32 permits visualization of the shear deformation field occurring in the mat during creeping of the foam. Shear deformation is located on shear band from the pile cap edges. Everywhere else the shear deformation is more or less zero. The maximum shear deformation is located at the pile cap edges and reaches 2%. For $H_M = 1.6s$, shear deformation is observed on a limited height in

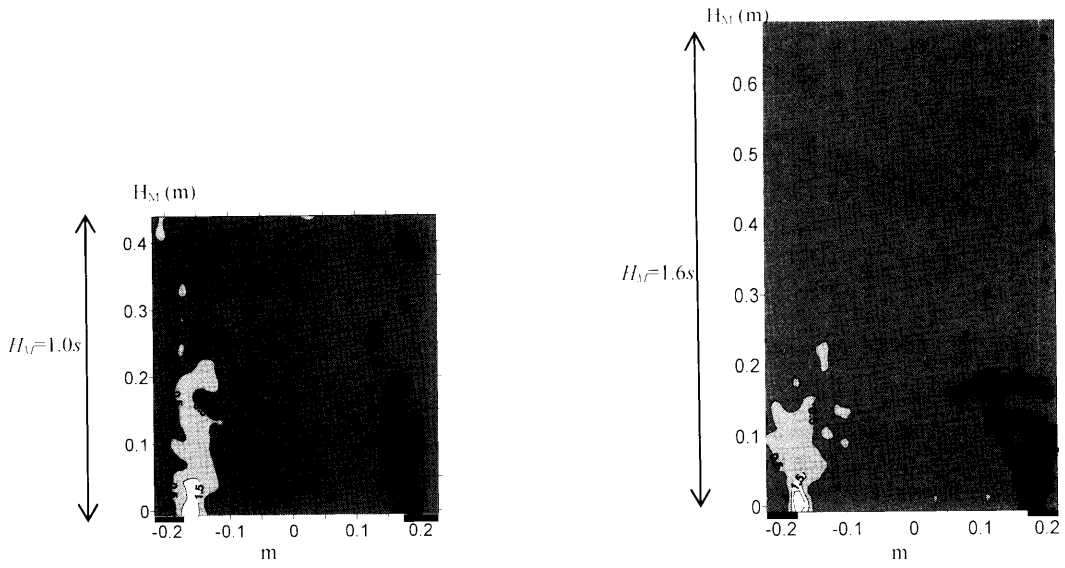

Fig. 32. Shear deformation (%) in the rod assembly during creeping of the foam for $\alpha = 22\%$

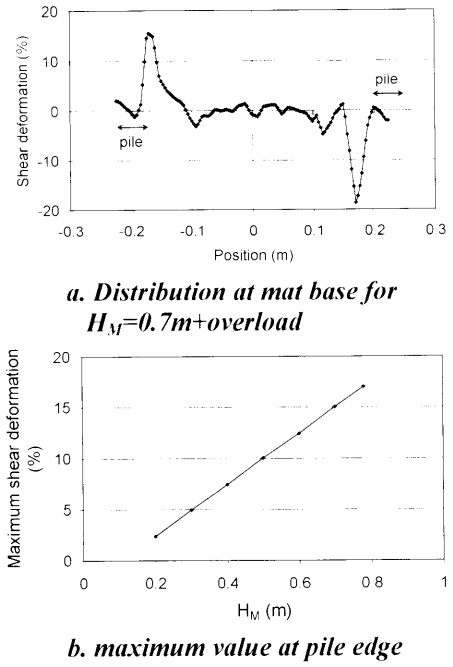

Fig. 33. Shear deformation at mat base

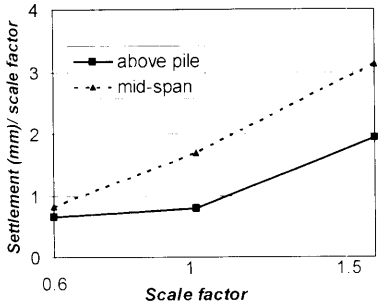

Fig. 34. Surface settlement during foam creeping, above the pile and mid-span

Table 2. Geometrical parameters for rod size influence analysis

Scale factor	a (m)	$s-a$ (m)	s (m)	$\alpha=a/s$	H_M	H_M/s
1.5	0.15	0.55	0.70	21%	0.70	1
1	0.10	0.35	0.45	22%	0.44	1
0.6	0.06	0.22	0.28	21%	0.28	1

the mat, showing that arching occurs. For $H_M = 1.0s$, the shear bands reach a greater value and are vertical, showing that full arching is not occurring.

Figure 33(a) depicts the distribution of the shear deformation at mat base for $H_M = 0.7$ m + overload. The maximum shear deformation is reached at pile edge. Everywhere else it is equal to zero. The evolution of this deformation according to mat height is depicted on Fig. 33(b). It increases linearly with H_M.

Influence of Rod Size

In order to study the effect of the relative size of the rods, three identical configurations were performed at different scales: pile caps of different size were used. The capping ratio and the maximum depth ratio H_M/s reached are equivalent (Table 2). For the test with $a = 0.15$ m, the rod size is 2.5 times smaller in comparison to the model test dimensions than for the test with $a = 0.06$ m.

Figure 34 depicts the settlements normalized by the scale factor occurring during foam creeping at mat surface. For a relatively large rod size (scale factor = 0.6), the surface settlement are small and homogenized,

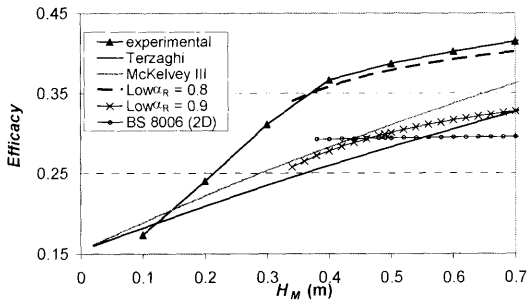

Fig. 35. Efficacy for $\alpha = 15\%$

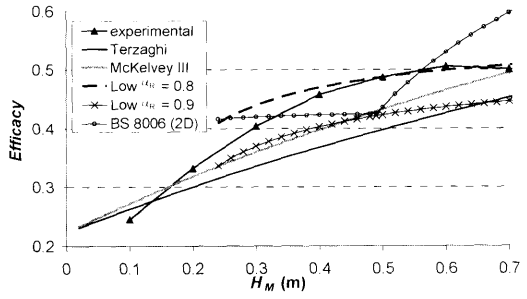

Fig. 36. Efficacy for $\alpha = 22\%$

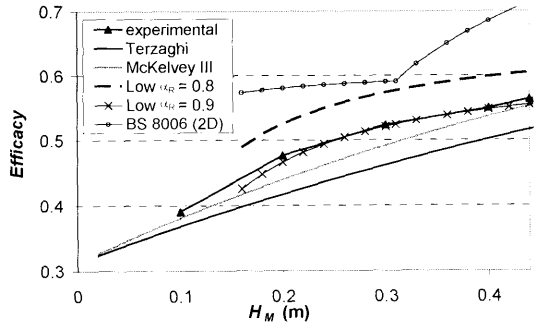

Fig. 37. Efficacy for $\alpha = 31\%$

whereas for smaller rod in comparison to model dimensions (scale factor = 1.5), the surface total and differential settlements increase. However, for a scale factor of 0.6, the mat height, thus the stress acting on the foam is smaller, and the foam is stiffer for stress weaker than 20 kPa (*see* Fig. 17).

PHYSICAL MODELLING VS DESIGN METHODS

In this part, experimental and two-dimensional design method results are compared in terms of stress distribution at mat base. The design methods used are:

—BS 8006 (1995) reformulated in two dimensions (after Marston and Anderson, 1913). Standards BS 8006 recommend $H_M > 0.7(s-a)$ and mentioned that all loads situated above the critical height $H_c = 1.4(s-a)$ are transferred directly to the pile caps. This critical height was determined for the 3D case.

—Terzaghi (1943) method adapted by Russel and Pierpoint (1997).

—The alternative to Terzaghi (1943) proposed by McKelvey III (1994).

—Low et al. (1994) method, using two different values for the coefficient α_R (0.8 and 0.9). This last method is applicable for $H_M > 0.5s$.

The calculation hypotheses are as follow:

$$\gamma = 62\ \text{kN/m}^3 \qquad \varphi_M = 24° \qquad c = 0\ \text{kPa}$$

$$K_a = \frac{1-\sin\varphi_M}{1+\sin\varphi_M} = 0.42 \quad K_p = 1/K_a = 2.37 \quad K_w = 0.53$$

In order to compare the methods between them and with the experimental results, the efficacy, proportion of the mat weight carried by the piles, is compared:

$$E = \frac{F_p}{W} = \frac{a}{s} \cdot \frac{q_p}{q^*} \tag{14}$$

Figures 35, 36 and 37 compare experimental results to calculation method results for a capping ratio of respectively 15%, 22% and 31% and a cap width of 0.1 m.

These figures show that Low method with $\alpha_R = 0.8$ for $\alpha = 15\%$ and 22%, and $\alpha_R = 0.9$ for $\alpha = 31\%$ is by far the most relevant when compared to experimental results. It accurately captures the measured evolution of E with H_M. However, this method is very sensitive to the empirical coefficient α_R and there is no way to accurately evaluate it. In fact this coefficient is arbitrary and its value was chosen to fit as good as possible to the experimental curve.

Terzaghi method and McKelvey III alternative method lead to efficacy values smaller than those determined experimentally. McKelvey III alternative method gives results closer to the experimental results than Terzaghi method. The comparison between both methods shows the sensibility to the K (K_a or K_w) parameter.

Adaptation of BS 8006 method in 2D does not give a variation of E with H_M in good agreement with the experimental results. In fact, this method does not explicitly take into account the mat material characteristics. Moreover, considering that all loads applied above a critical height of $H_c = 1{,}4\ (s-a)$ are directly transferred to the piles gives inconsistent results: efficacy is strongly overestimated when H_M rises. The 2D adapted BS 8006 method overestimates the efficacy for $\alpha = 31\%$ and underestimates it for $\alpha = 15\%$.

CONCLUSIONS AND PERSPECTIVES

A two dimensional physical model permitted us to study the load transfer mechanisms that take place in the granular mat. As the similarity between model and prototype is not strictly maintained, the experimental results are more qualitative than quantitative. The results can not be directly extrapolated to real structures, but they can be used as a database for numerical approaches or they can be confronted to design methods in order to estimate their validity.

The numerical imaging technique proves to be effective

for the displacement field analysis.

The parametric study highlights the conjoined influence of the capping ratio and the mat height on the arching mechanisms. The physical modelling clearly shows a reduction of total and differential settlements in the mat when capping ratio and depth ratio increase, especially at the mat surface. It was shown that full arching occurs for a mat height of 1.6 times the pile spacing, whereas shear planes extend to the surface for a mat height equal to the pile spacing. The proportion of the mat weight supported by the piles increases with the mat height. It reaches a threshold value from a mat height of about 1.5 times the pile spacing. When the pile caps are spaced further, the load that they carry becomes larger, but the proportion of the total load that they carry becomes smaller. The rod size influence was also highlighted. The arching effect seems to be more efficient for greater rod size in comparison to the geometrical dimensions.

The confrontation of test results to calculation rules shows a good agreement in the case of Low et al. (1994) method, for different values of the empirical coefficient α_R depending on the capping ratio. However, this method is very sensitive to this empirical parameter. The result differences between Terzaghi and McKelvey III methods show their sensitivity to the K parameter (K_a or K_w). BS 8006 method does not seem appropriate to our two-dimensional problem and it does not take into account the angle of friction of the mat material.

On the base of the constituted experimental database, further works are being done now to numerically model the experiment with help of a continuum mechanic software, using constitutive laws adapted to analogical soil behaviour, and also with a discrete element method.

This study is part of a new French national project in which field experiments, centrifuge modelling and 3D numerical modelling are also planned. The mechanical behaviour of granular earth platform soil will be investigated by laboratory tests in order to determine the rheological model parameters.

NOTATION

A_p Pile cap section
C Competency
C_c Arching Coefficient (Marston and Anderson, 1913)
E Efficacy
F_p Pile cap load
F_s Load acting on the surface of the foam
F_b Load acting on the foam element support
F_{lt} Friction (force) along lateral boundaries of a rigid element
H_M Mat height
$H_M/(s-a)$ Depth ratio
H_c Critical height
K_a Coefficient of active lateral earth pressure
K_p Coefficient of passive lateral earth pressure
K_w Handy's (1985) coefficient
SRR Stress reduction ratio
SRR_m Modified SRR
W Mat weight
a Pile cap width
c Cohesive strength of the mat soil
d Circular pile cap diameter
d_E Equivalent non circular pile cap diameter
dh Thickness of a particular soil element
f Function of grey level in the initial picture
f^* Function of grey level in the deformed picture
l Length of the Schneebeli rods
q^* Vertical stress acting on non reinforced subsoil
q_0 Surface overload
q_s Vertical stress acting on subsoil, when reinforced by piles, above the geosynthetic
q_b Average vertical stress acting on the foam rigid support
q_p Vertical stress acting on a pile cap
s Pile spacing
s_m Maximum pile spacing (3D grid)
$s\%$ Reduction of settlement in percentage
s_p Foam settlement in the case of pile improvement
s^* Foam settlement without pile improvement
u Horizontal displacement
v Vertical displacement
α Capping ratio
ε Strain
γ Mat unit weight
φ_M Friction angle of mat soil
α_R Stress reduction coefficient in Low et al. (1994) method
σ_3 Confinement pressure
σ_h Horizontal stress
σ_v Vertical stress
τ Shear stress

REFERENCES

1) Alexiew, D. and Vogel, W. (2002): Remblais ferroviaires renforcés sur pieux en Allemagne: projets phares, *Travaux*, **786**, 47–52.
2) Barry, A. J., Trigunarsyah, B., Symes, T. and Younger, J. S. (1995): Geogrid reinforced piled road over peat, *Engineering Geology of Construction*, The Geological Society, London, 205–210.
3) Berthelot, P., Pezot, B. and Liausu, Ph. (2003): Amélioration des sols naturels ou anthropiques par colonnes semi-rigides: le procédé CMC, *XIII CMSGE*, Prague.
4) Briançon, L. (2002): Renforcement des sols par inclusions rigides-Etat de l'art en France et à l'étranger, *IREX*, 185.
5) Briançon, L., Kastner, R., Simon, B. and Dias, D. (2004): Etat des connaissances: Amélioration des sols par inclusions rigides, *ASEP-GI 2004*, Paris, 15–43.
6) BS 8006 (1995): Code of practice for strengthened/reinforced soils and other fills, *Section 8*, British Standard Institution.
7) Collin, J. G., Watson, C. H. and Han, J. (2005): Column-supported embankment solves time constraint for new road construction, *Geo-Frontiers 2005*.
8) Combarieu, O. (1988): Amélioration des sols par inclusions rigides verticales. Application à l'édification de remblais sur sols médiocres, *Revue Française de Géotechnique*, **44**, 57–79.
9) Cortlever, N. G. (2001): Design of double track railway on AuGeo piling system, *Symp. 2001 on Soft Ground Improvement and Geosynthetic Applications*, AIT, Bangkok.
10) Demerdash, M. A. (1996): An experimental study of piled embankments incorporating geosynthetic basal reinforcement, *Thesis*, University of Newcastle-upon-Tyne.
11) Dolzhenko, N. (2002): Etude expérimentale et numérique de modèle réduit bidimensionnel du creusement d'un tunnel, *Thèse de Doctorat*, INSA de Lyon, Villeurbanne.
12) EGBEO (2004): Bewehrte Erdkörper auf punkt- und linienförmigen Traggliedern, *Entwurf Kapitel 6.9, 05/16/2004 version*, non published.
13) FOXTA (2004): Manuel d'utilisation v2.0, Terrasol.
14) Habib, H. A. A., Brugman, M. H. A. and Uijting, B. G. J. (2002): Widening of road N247 founded on a geogrid reinforced mattress on piles, *7th ICG*, Nice, France, 369–372.
15) Handy, R. L. (1985): The arch in arching, *J. Geotech. Engrg.*,

111(50), 302–317.
16) Hewlett, W. J. and Randolph, M. F. (1988): Analysis of piled embankment, *Ground Engrg.*, **21**(3), 12–18.
17) James, R. G. (1972): Some aspects of soil mechanics model testing, *Stress-strain Behaviour of Soils, Roscoe Memorial Symp.*, Cambridge, UK, 417–440.
18) John, N. W. M. (1987): Geotextiles, *Chapman and Hall, New York, Blackie.*
19) Jones, C. J. F. P., Lawson, C. R. and Ayres, D. J. (1990): Geotextile reinforced piled embankments, *4th Int. Conf. Geotextiles Geomembranes and Related Products*, Den Haag, **1**, 155–160.
20) Kempfert, H. G., Stadel, M. and Zaeske, D. (1997): Berechnung von geokunststoffbewehrten Tragschichten über Pfahlelementen, *Bautechnik*, **74**(12), 818–825.
21) Laurent, Y., Dias, D., Simon, B. and Kastner, R. (2003): A 3D finite difference analysis of embankments over pile-reinforced soft soil, *Int. Workshop Geotech. of Soft Soils*, Noordwijkerhout, The Netherlands, 271–276.
22) Liausu, Ph. and Pezot, B. (2001): Renforcement de sols mous par colonnes à module contrôlé, *15th ICSMGE*, Istanbul, **2**, 1613–1618.
23) Love, J. P. and Milligan, G. W. E. (2003): Design methods for basally reinforced pile supported embankments over soft ground, *Ground Engrg.*, March 2003, 39–43.
24) Low, B. K., Tang, S. K. and Choa, V. (1994): Arching in piled embankments, *J. Geotech. Engrg.*, **120**(11), 1917–1937.
25) Magnan, J. P. (1994): Methods to reduce the settlement of embankments on soft clay: a review, *Spec. Conf. Found. Embank. Deform.*, ASCE, (Geotech. Spec. Pub. n° 40), 77–90.
26) Mankbadi, R., Mansfield, J., Wilson-Fahmy, R., Hanna, S., and Krstic, V. (2004): Ground improvement utilizing vibro-concrete columns, *GeoSupport Conf. 2004*, Orlando, USA.
27) Marston, A. and Anderson, A. O. (1913): The theory of loads on pipes ditches and tests of cement and clay drain tile and sewer pipes, *Iowa Eng. Exp. Station Armes*, bull. 31.
28) McKelvey III, J. A. (1994): The anatomy of soil arching, *Geotextiles and Geomembranes*, **13**(5), 317–329.
29) Mguil-Touchal, S., Morestin, F. and Brunet, M. (1996): Mesure de champs de déplacements et de déformations par corrélation d'images numériques, *Mécamat'96*, Aussois, France, 179–182.
30) Naughton, P. J. and Kempton, G. T. (2005): Comparison of analytical and numerical analysis design methods for piled embankments, *Geo-Frontiers 2005*, Austin, USA.
31) Paute, J.-L., Hornych, P. and Benaben, J.-P. (1994): Comportement mécanique des graves non-traitées, *Bull. de Liaison des Ponts et Chaussées*, **190**, 27–38.
32) Rathmayer, H. (1975): Piled embankment supported by single pile caps, *Conf. Soil Mech. Found.*, Istanbul.
33) Rogbeck, Y., Gustavsson, S., Soedergren, I. and Lindquist, D. (1998): Reinforced piled embankments in Sweden–Design aspects, *6th ICG*, 755–762.
34) Russell, D. and Pierpoint, N. (1997): An assessment of design methods for piled embankments, *Ground Engrg.*, November, 39–44.
35) Russell, D. and Pierpoint, N. (1998): Assessment revisited. Author's response, *Ground Engrg.*, 47–50.
36) Russell, D., Naughton, P. and Kempton, G. (2003): A new design procedure for piled embankments, *56th Annu. Can. Geotech. Conf.*, Winnipeg, Canada.
37) Schneebeli, G. (1956): Une mécanique pour les terres sans cohésion, *Compte rendus des séances de l'Académie des Sciences*, tome 243, 2647–2673.
38) Simon, B. (2001): Une Méthode intégrée pour dimensionner les réseaux d'inclusions rigides en déformation, *15th ICSMGE*, Istanbul, **2**, 1007–1010.
39) Stewart, M. E. and Filz, G. M. (2005): Influence of clay compressibility on geosynthetic loads in bridging layers for column-supported embankments, *Geo-Frontiers 2005*, Austin, USA.
40) Terzaghi, K. (1943): *Theoretical Soil Mechanics*, John Wiley & Sons, New York.
41) Valle, N. (2001): Comportement mécanique d'un sol grossier d'une terrasse alluvionnaire de la Seine, *Thèse de doctorat, Université de Caen/Basse Normandie.*
42) Van Eekelen, S. J. M., Bezuijen, A. and Oung, O. (2003): Arching in piled embankments, experiment and design calculation, *BGA Int. Conf. Found.*, Dundee, 889–894.
43) Wood, H. J. (2003): The design and construction of pile-supported embankments for the A63 Selby Bypass, *BGA Int. Conf. Found.*, Dundee, 941–950.
44) Zanziger, H. and Gartung, E. (2002): Performance of a geogrid reinforced railway embankment on piles, *7th ICG*, Nice, France, 381–386.